Continuous-electron-beam focusing induced by collective plasma interactions in D_2 and H_2

F. Giammanco
Dipartimento di Fisica, Università di Pisa, Piazza Torricelli 2, 56126 Pisa, Italy

M. Armenante
Dipartimento di Fisica, Università di Napoli, I-80125 Napoli, Italy

V. Berardi, N. Spinelli, and R. Velotta
Dipartimento di Scienze Fisiche, Università di Napoli, Padiglione 20, Mostra d'Oltremare, Napoli, Italy
(Received 10 August 1992)

An experimental analysis of the focusing of a continuous electron beam, induced by the mutual interaction with charges produced by electron impact, is presented. The phenomenon has been observed by measuring the beam current on two different detector active areas as a function of the gas pressure in H_2 and D_2. The stationary solutions of a three-fluid model, already developed, allow us to measure the maximum beam density. Moreover, we carry out information about the main processes responsible for ionization and their cross sections in the case of a three-component quasiequilibrium plasma.

PACS number(s): 52.25.Wz, 34.80.Dp

I. INTRODUCTION

Collective effects, depending on the electron-ion mutual interaction, have been recently highlighted and analyzed in experiments where ionization of the gaseous sample was produced by laser-induced multiphoton interaction or by collision with an electron beam [1–3]. Particularly, relevant collective effects, consisting in a noticeable ion and electron-beam focusing as a function of the gas pressure, were observed in a low-density molecular gas (pressure 10^{-6}–10^{-4} torr) ionized by a pulsed electron beam, whose duration, energy, and intensity were 10 ns, 40 eV, and 10 nA, respectively [2].

The increase of the peak and of the total charge of the electron-beam current, after it has passed through the target gas, was observed in a very narrow range of pressure variation. A similar sudden change in slope was observed for the total ion count rate in the same range of pressure variation.

Basically, the phenomenon depends on the different mobility of the involved charged species, i.e., incident and produced electrons, and ions. The produced electrons leave the interaction zone, as an effect of their initial kinetic energy, so that a positive internal field, due to the ions at rest, grows up, stops the electron expansion, and reverses the electron motion. Therefore, incident and produced electrons are focused and their local density overcomes the ionic one, because of the excess of negative charges due to the incident beam, in such a way that ions too begin to be focused.

As pointed out in Ref. [2], the efficiency of the process depends mainly on the expansion of secondary electrons which leads to the growth of a positive-ion field. A quantitative description of the phenomenon, whose main features are briefly recalled in Sec. III, has been given in Ref. [2] by means of the three-fluid-equation system.

The time scale of secondary electron expansion depends on their initial kinetic energy, and on the width of the interaction zone. In order to observe the focusing effect, this time scale must be shorter than the pulse duration.

In this work, we report on the continuous-electron-beam focusing in the presence of a uniform background of D_2 or H_2 gas, and in the case of gas injected by a needle, whose diameter is 500 μm, which introduces a local overpressure.

The total electron charge has been measured for two active areas of the detector. By combining both electron charge's dependences on the gas pressure, and by using the stationary solution of the model, we carry out the value of the maximum electron-beam density, and the rate of ionization. Moreover, the deduced rate of ionization, in H_2 and D_2, allows us to evaluate the main elementary processes involved in the ionization of gas. By the same technique, we obtain the value of the overpressure due to the needle. Finally, we discuss the experimental conditions in order to achieve focusing of a continuous electron beam.

II. EXPERIMENTAL SETUP

Figure 1(a) shows the experimental apparatus mainly consisting in the electron gun, which includes an indirectly heated oxide cathode and two electrostatic lenses [2], and the detector in front of it, at a distance of 8 cm, placed in a cylindrical vacuum chamber whose diameter and height are 40 and 15 cm, respectively. The residual pressure is 3×10^{-8} torr. A spatially integrated imaging of the beam is obtained by a detector, whose head is constituted by five electrodes, as Fig. 1(b) shows.

In order to evaluate the effects of the density gradient, according to the model of Ref. [2], we compare the dependence of the current on the pressure when the gas is uniformly distributed into the vacuum chamber, and

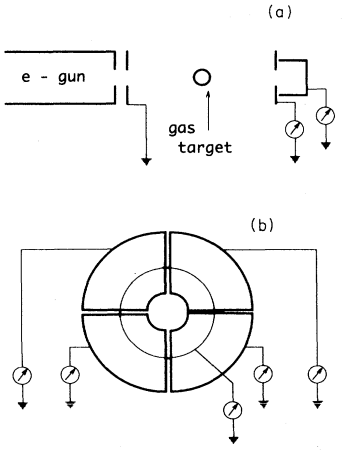

FIG. 1. (a) Experimental setup. (b) Details of the detector head.

when the gas is injected by a needle, whose diameter is 500 μm, inserted in the region between the electron gun and the detector. In the second case, the needle introduces a local overpressure, whose value is about a factor of 10 greater than the background one (Sec. IV).

We measure the transmitted current on the central electrode (I_d), whose diameter is 0.3 cm, and on the four surrounding electrodes (I_T) [Fig. 1(b)], whose external diameter is 2.5 cm, as a function of the gas pressure in the range 10^{-7}–10^{-4} torr, for two different beam energies, i.e., 40 and 100 eV, and for H_2 and D_2.

III. THEORETICAL MODEL

According to Refs. [3] and [4], the three-fluid approximation constitutes a suitable approach to describe the time-space evolution of charges. In fact, it is sufficient an isotropic velocity distribution to make the fluid scheme valid. The basic equations describe the time-space evolution of the fluid mean quantities (velocity, density, and temperature) referred to the laboratory frame. The fluid velocity represents the average component of collective motion, whereas the temperature is related to the mean kinetic energy of random motion of the particles. Thus, the energy conservation includes two terms, representing the internal energy of the fluid, function of the temperature, and the mean kinetic energy of the fluid collective motion. Therefore, the basic equations are given by

$$\frac{\partial \mathbf{v_j}}{\partial t}+(\mathbf{v_j}\cdot\nabla)\mathbf{v_j}=\frac{e_j}{m_j}\mathbf{E_r}-\frac{1}{n_j}\nabla\left[\frac{kT_j}{m_j}n_j\right], \tag{1}$$

$$\frac{\partial n_j}{\partial t}+\nabla\cdot(n_j\mathbf{v_j})=S_j, \tag{2}$$

$$\frac{\partial U_j}{\partial t}+(\mathbf{v_j}\cdot\nabla)U_j-kT_j\frac{\partial \ln(n_j)}{\partial t}+(\mathbf{v_j}\cdot\nabla)kT_j=e_j\mathbf{v_j}\cdot\mathbf{E_r}, \tag{3}$$

$$\frac{\partial kT_j}{\partial t}+(\mathbf{v_j}\cdot\nabla)kT_j+\tfrac{2}{3}kT_j(\nabla\cdot\mathbf{v_j})=0, \tag{4}$$

where $\mathbf{v_j}$, e_j, m_j, and n_j are the collective velocity, charge, mass, and density of the involved species, respectively. $\mathbf{E_r}$ represent the self-generated electric field given by the Poisson equation. The term $e_j\mathbf{v}_j\cdot\mathbf{E}_r$ takes into account the energy exchange per particle due to the self-generated field. S_j represents the source term responsible for the growth of ionization. U_j is the total average charged particle energy, i.e., $U_j=\frac{1}{2}mv_j^2+\frac{1}{2}m\langle w_j^2\rangle$. The first term is the kinetic energy associated with the mass (collective) motion of the gas and the second is the average kinetic energy of a particle. Hence, for the incident beam, the first term corresponds to the beam energy, whereas the second term represents the beam thermal spread [2]. In the system of Eqs. (1)–(4) we neglect the two-body collisions because of the low charge density range of investigation.

A solution to the system can be found by using the approach developed in Refs. [3] and [4], based on an analysis of the time-space evolution of an initially produced Gaussian-shaped profile of charges. In the following, the technique of solution is briefly recalled, and applied to reduce the partial derivative system of Eqs. (1)–(4) to a total time derivative system of coupled equations.

In the simplest case, i.e., assuming $E_r=0$ and $U_e\approx kT_e$ constant and uniform, and negligible ionization time for charges produced by electron impact, motion is still represented by a Gaussian-shaped profile, whose width is a function of time. Thus the one-dimensional time-space evolution of the density profile along the x axis is expressed as

$$n_j(x,t)=n_0 f_{j,x}(t)^{1/2}\exp[-f_{j,x}(t)x^2/d_{j,x}^2], \tag{5}$$

where $d_{j,x}$ and n_0 represent the initial charge distribution width and density of the j species, respectively. The continuity equation provides the functional dependence of the fluid mean velocities on n_j and, thus, on the $f_{j,x}(t)$ function, namely

$$v_e=-\frac{x}{2}\{D\ln[f_x(t)]\}. \tag{6}$$

The function $f_{j,x}(t)$ satisfies initial conditions $f_{j,x}(t=0)=1$, and $Df_{j,x}(t)|_{t=0}=0$. A second-order differential equation describing the $f_{j,x}(t)$ time evolution is derived form the motion equation by replacing the n_j and v_j dependences on $f_{j,x}(t)$, and by equating the terms with the same power dependence on the spatial coordinates.

Due to the independence of motion along the axes, the three-dimensional motion is represented by a product of three Gaussian profiles with different initial widths, depending on the symmetry of the charges production. Thus the time evolution of $f_{j,k}(t)$ ($k=x$, y, and z) along any axes depends on the initial width $d_{j,k}$. Therefore, in the cylindrical symmetry, as in the present experiment, we can neglect the expansion along the beam direction, and Eq. (5) becomes

$$n_j(r,t)=n_0 f_{j,r}(t)\exp[-f_{j,r}(t)r^2/d_{j,r}^2] \tag{7}$$

where r is the radial coordinate.

In general, the previous scheme does not hold if applied to the complete system. Nevertheless, if all terms can be expressed in a form such as $G(t)+F(t)\mathbf{r}$, where $\mathbf{r}=(x,y,z)$, the basic scheme of solution still holds true. Hence the Poisson equation is linearized around the coordinate of the single-particle-like motion for electrons, i.e., around the top of the Gaussian profiles [3,4]. Since we are dealing with a stationary motion, ions can be assumed at rest, i.e., the ion local density is simply given by the balance between electron-impact ionization and loss terms. Hence we assume $f_{i,r}(t)=1$.

For the sake of simplicity, the model is developed for the case of diffuse gas, which implies an equal width d_r for secondary and incident electrons, since the extension to the case of gas injected by a needle is straightforward, once the technique of solution is established. According to Refs. [3] and [4], the internal field is given by

$$E_r(r,t)=4\pi e[N_s(1-f_s)-n_{0p}f_p]r \ , \tag{8}$$

where N_s, f_s, n_{0p} and f_p are density and f functions of the secondary charges produced by electron impact, and of the incidence beam, respectively.

Equation (8) is valid insofar as the second term of the series development of the electric field is negligible [3]. Thus the spatial interval of validity of Eq. (8) is given by the condition

$$\left[\frac{r_{\lim}}{d_r}\right]^2 \le \frac{3|\alpha_s(1-f_s^{1/2})-f_p^{1/2}|}{|\alpha_s(1-f_s^{3/2})-f_p^{3/2}|} \ , \tag{9}$$

where $\alpha_s=N_s/n_{0p}$.

According to the approximations of Ref. [3], the radius deduced from Eq. (9) defines a sharp boundary between the fluid motion of charges coupled by the self-generated field and the single-fluid expansion of each species. Therefore the beam density can be represented as

$$n_p(r,t)=n_{0p}f_p(t)\exp[-f_p(t)r^2/d_r^2] + k(t)n_{0p}f_f(t)\exp[-f_f(t)r^2/d_r^2] \ , \tag{10}$$

where n_{0p} is the initial beam density, and f_p and f_f are the f functions of the beam in the coupled and uncoupled region, whose boundary $r_{\lim}$ is given by Eq. (9).

The fraction $k(t)$ of particles in the uncoupled region is given by the integral equations [3]

$$n_{0p}f_p\int_0^{r_{\lim}}\exp\left[-\frac{f_p r^2}{d_r^2}\right]2\pi r\,dr + k(t)n_{0p}f_f\int_{r_{\lim}}^{\infty}\exp\left[-\frac{f_f r^2}{d_r^2}\right]2\pi r\,dr = n_{0p}\pi d_r^2 \tag{11}$$

and, after integration,

$$k(t)=\exp\left[(f_f-f_p)\left[\frac{r_{\lim}}{d_r}\right]^2\right] \ . \tag{12}$$

Hence the beam current I is obtained by integrating Eq. (10) on a surface of the detector, whose radius is R_D. If $r_{\lim}\ge R_D$, i.e., the detector area is internal to the coupled zone, the beam current is given by

$$I=en_{0p}v_{0p}\pi d_r^2[1-\exp(-f_pR_D^2/d_r^2)] \tag{13}$$

and, in the case of $r_{\lim}<R_D$, I becomes

$$I=en_{0p}v_{0p}\pi d_r^2 \times\left\{1-\exp(-f_fR_D^2/d_r^2)\exp\left[(f_f-f_p)\left[\frac{r_{\lim}}{d_r}\right]^2\right]\right\} , \tag{14}$$

where v_{0p} is the beam velocity.

In the stationary case, the second-order differential equations for the f functions [3], in the coupled zone, of incident and produced electrons, i.e., f_p and f_s, respectively, become

$$\tfrac{2}{3}\omega_s^2(1-f_s)-2B_pf_p^{5/3}-\tfrac{2}{3}\omega_p^2f_p=0 \ , \tag{15}$$

$$\tfrac{2}{3}\omega_s^2(1-f_s)-2B_sf_s^{5/3}-\tfrac{2}{3}\omega_p^2f_p=0 \ , \tag{16}$$

where $\omega_s^2=4\pi e^2N_s/m$ and $\omega_p^2=4\pi e^2n_{0p}/m$ are the plasma frequencies due to produced and incidence electrons, respectively. The B coefficients represent the expansion due to the average kinetic energy of random motion of particles, i.e., $B_s=2kT_{0s}/(md_r^2)$ and $B_p=2kT_{0p}/(md_r^2)$, where T_{0s} and T_{0p} ar the initial average kinetic energy of produced electrons and the initial thermal spread of the beam, respectively. In the system of Eqs. (15) and (16), we take into account that Eq. (4) relates the temperature to the charge density by an adiabatic relation. In the absence of collisions and temperature gradients, as in the present experiment, then $T(t)=T_0(f_xf_yf_z)^{1/3}$, which under hypothesis of radial expansion becomes $T(t)=T_0f^{2/3}$ [4].

From the system of Eqs. (15) and (16), it turns out that $f_s=(T_{0p}/T_{0s})^{3/5}f_p$. Hence the ratio of ionization α_s is related to f_p by

$$\alpha_s=\frac{\beta_pf_p^{5/3}+f_p}{1-\xi f_p} \ , \tag{17}$$

where $\beta_p=2B_p/\omega_p^2$ and $\xi=(T_{0p}/T_{0s})^{3/5}$. Equation (17) gives the maximum beam density achievable in this configuration, i.e., $f_p=1/\xi=(T_{0s}/T_{0p})^{3/5}$, which corresponds to the condition $\alpha_s\gg1$. It turns out that the maximum value of f_p depends on the ratio of the radial expansion of produced and incident charges, and hence on the ratio of the temperatures. As the rate of radial expansion for produced electrons increases, the electric field due to ions is less neutralized, and then the incident electrons experience a stronger focusing.

Finally, the value of f_f is given by integration of the differential equation without the coupling term due to the produced charges, namely [3]

$$D^2f_f=\frac{3(Df_f)^2}{2f_f}-2B_pf_f^{8/3}-\tfrac{2}{3}\omega_p^2f_f^2 \ . \tag{18}$$

The integration time is given by the transit time from the cathode of the electron gun to the detector.

The limit of validity of the assumption of ions at rest, i.e., $f_{i,r}(t)=1$, can be analyzed in the framework of the system of Eqs. (15) and (16). Actually, the stationary equation for ions, obtained by the transformation $m \equiv M$, $T_{0s} \equiv T_i$, with M and T_i ion mass and temperature, respectively, and by sign inversion of the term related to the self-consistent field, should be added to the system. In such a case, the only stationary solution should be $f_i = f_s = f_p = 0$, which corresponds to the asymptotic evolution of charges in the absence of ionizing sources. In the present case, ionization of gas occurs continuously, and hence the ion density is only determined by the local balance among elementary processes (ionization and recombination), if the time scale of ion expansion due to thermal motion and/or to Coulombian repulsion is negligible during the transit time of the electron beam from the gun to the detector. It turns out that the focusing condition is approximately given by

$$\min\left\{\frac{M}{4\pi e^2 N_s(1-f_s)}, \frac{d_r^2 M}{2kT_i}\right\} \gg \frac{L^2}{v_{0p}^2}, \tag{19}$$

where L is the distance between the electron gun and the detector, and the other symbols have been already defined.

In our case, with $L=8$ cm and a maximum ion density $\approx 4\times 10^9$ ion/cm^3 (Sec. IV), Eq. (19) is always satisfied. It turns out that the ion density must fulfill simultaneously the above-mentioned condition $N_s \gg n_{0p}$, and Eq. (219), in order to achieve the maximum electron-beam focusing.

In the case of gas injected by a needle, the scheme of solution holds true providing that the additional contribution to the ionization be introduced in Eq. (8). It turns out that the boundary of the coupled zone is given by

$$\left[\frac{r_{\lim}}{d_r}\right]^2 \leq \frac{3|\alpha_s(1-f_s^{1/2})-f_p^{1/2}|+3|\alpha_{sN}(1-f_{sN}^{1/2})|d_r/d_N}{|\alpha_s(1-f_s^{3/2})-f_p^{3/2}|+|\alpha_{sN}(1-f_{sN}^{3/2})|(d_r/d_N)^3}, \tag{20}$$

where $\alpha_{sN}=N_{sN}/n_{0p}$, f_{sN}, and d_N are the ratio of ionization, the coupled f function, and the width of the needle, respectively. By adding to Eqs. (15) and (16), the equation for f_{sN}, it turns out that $f_{sN} = (T_{0p}/T_{0s})^{3/5}(d_N/d_r)^{6/5} f_p$, and then

$$\alpha_{sN} = \frac{\beta_p f_p^{5/3} + f_p - \alpha_s(1-\xi f_p)}{1-\xi_N f_p}, \tag{21}$$

where $\xi_N = (T_{0p}/T_{0s})^{3/5}(d_N/d_r)^{6/5}$. In this case, the maximum beam density is achieved when $f_p = 1/\xi_N = (T_{0s}/T_{0p})^{3/5}(d_r/d_N)^{6/5}$. It turns out that the ratio of density gradients, proportional to d_r/d_N, introduces an additional focusing in the case of needle, because the produced electrons leave the interaction zone faster, as pointed out in Ref. [2]. Moreover, owing to the local overpressure due to the needle, it is possible to saturate the ratio of ionization, and hence to achieve the maximum focusing, without an increase of the background pressure in the chamber.

Recalling Eqs. (12) and (20), for $\alpha_{sN} \gg 1$, the fraction of untrapped particles becomes $k(t) \approx \exp[-3(T_{0s}/T_{0p})^{3/5}(d_N/d_r)^{4/5}]$, where $f_p \gg f_f$. In our case, with $T_{0s} \approx 2$ eV [2], $T_{0p} \approx 0.2$ eV, $d_r = 0.1$ cm, and $d_N = 0.05$ cm, $k(t) \approx 0.001$. It turns out that the most important part of the beam is focused by the ion field in spite of the smaller dimensions of the needle. Moreover, the condition of Eq. (19) is fulfilled also in the case of total ionization of gas, in our range of investigation, due to the needle length along the beam direction, which implies a transit time much shorter than in the case of diffuse gas.

IV. EXPERIMENTAL RESULTS

The electron current has been measured on a surface detector diameter of 0.3 cm (I_d) and 2.5 cm (I_T), respectively. Figures 2 and 3 show a typical behavior of the beam current in D_2 and H_2 as a function of the gas pressure, with a beam energy 100 eV, and diffuse gas.

Since the diameter of the smaller surface is equal to the aperture of the electron gun, the low-pressure measurements with the largest surface show that the beam divergence is higher than that simply due to the beam thermal

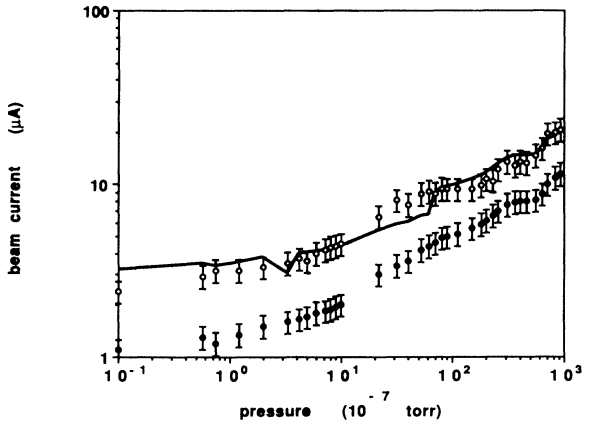

FIG. 2. D_2 diffuse gas. Electron-beam energy 100 eV. (a) Open circles I_T. (b) Black circles I_d. Solid line is the best fit of I_T, deduced from data of I_d with $n_{0p} = 4\times 10^7$ electrons/cm^3.

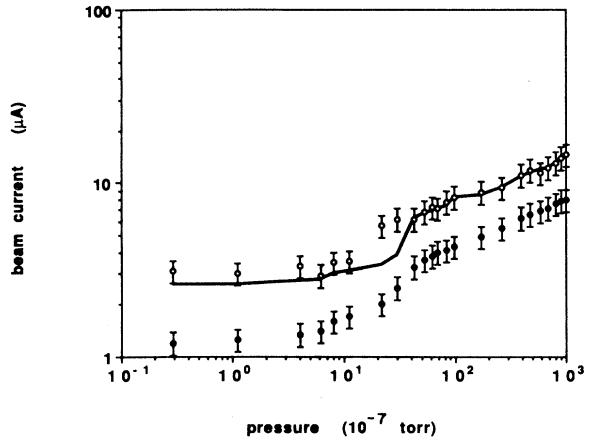

FIG. 3. H_2 diffuse gas. Electron-beam energy 100 eV. (a) Open circles I_T. (b) Black circles I_d. Solid line is the best fit of I_T, deduced from data of I_d with $n_{0p}=4\times10^7$ electrons/cm^3.

spread [B_p in Eq. (18)], otherwise I_T should be less sensitive to the pressure variation. Hence the Coulombian repulsion plays a relevant role, and the lowest value of the beam density can be calculated by the equating second and third term of Eq. (18), with $f=1$. Starting from this value, we deduce f_p from the experimental values of I_d, by using Eq. (13) or (14), according to the condition of Eq. (9), with $R_D=0.15$ cm. Once calculated f_p, we try to fit the experimental values of I_T, by using eq. (13) or (14), with f_f corresponding to the selected value of n_{0p}, and $R_D=1.25$ cm.

Once I_T is fitted by a proper choice of the beam density n_{0p} (solid lines of Figs. 2 and 3), we obtain immediately the ratio α_s between the produced charge density and

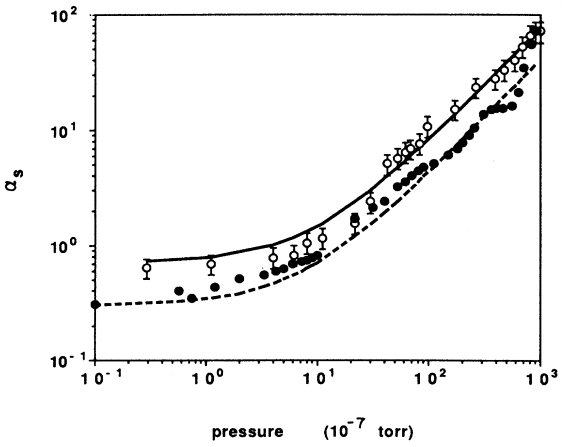

FIG. 4. Ratio α_s between the produced charge density and the electron-beam density $n_{0p}=4\times10^7$ electrons/cm^3 vs pressure, for diffuse gas. Electron-beam energy 100 eV. Black circle values deduced from data of Fig. 2 for D_2. Dashed line is the best linear fit, i.e., $\alpha_s=0.3+4\times10^{-2}\mathcal{P}$, where $\mathcal{P}$ is in units 10^{-7} torr. Open circle values deduced from data of Fig. 2 for H_2. Solid line is the best linear fit, i.e., $\alpha_s=0.7+7.5\times10^{-2}\mathcal{P}$.

n_{0p}, and f_p, as a function of the gas pressure. The value of n_{0p}, corresponding to the solid lines of Figs. 2 and 3, is 4×10^7 electrons/cm^3 with a confidence of 20%. Moreover, the deduced beam parameters allow us to fit the current behavior measured in H_2 and D_2 with 40-eV electron-beam energy. Then it confirms self-consistence of the theoretical model.

Figure 4 shows the α_s values as a function of the gas pressure for H_2 (open circles) and D_2 (black circles), for diffuse gas and an electron-beam energy of 100 eV, deduced from data of Figs. 2 and 3. α_s values are given with a confidence of 20%, which accounts for experimental errors in measuring the beam current. f_p ranges from 0.1 at $P=10^{-8}$ torr to 1.4 at $P=10^{-4}$ torr for H_2, and f_p is a factor of 2 less for D_2, except for pressures around 10^{-4} torr where f_p approaches the maximum value for H_2.

The value of f_f is 10^{-3}, from Eq. (18) with $n_{0p}=4\times10^7$ electrons/cm^3. Hence the beam focusing begins to be effective even for a very low value of proposed charge density, i.e., $\approx3\times10^7$ electrons/cm^3. Nevertheless, f_p does not reach $f_{p\max}=(T_{0s}/T_{0p})^{3/5}\approx4$, where $T_{0s}=2$ eV, and $T_{0p}=0.2$ eV. Then, a produced charge density about 4×10^9 electrons/cm^3 ($\alpha_s\approx10^2$) is not yet sufficient to achieve in this configuration the maximum beam focusing. However, the beam density increase due to the ionization is about 1.4×10^3 times compared with the free expansion in vacuum. In the case of gas injected by needle, $f_p\approx8$, i.e., f_p approaches $f_{p\max}=(T_{0s}/T_{0p})^{3/5}(d_r/d_N)^{6/5}\approx9.2$ due to the gas overpressure which increases the degree of ionization (see below).

Figure 4 shows a mass dependence of α_s in favor of H_2 which disappears at 10^{-4} torr, in apparent disagreement with values of the cross sections for direct electron-impact ionization of H_2 and D_2 measured by several authors [5,6]. However, in the stationary case the charge density is given by the balance among competing processes as direct ionization, recombination, and formation of ionized molecular compounds.

The α_s dependences on the gas pressure are fitted well by a linear function $a+bP$. Solid line represents the best linear fit for H_2, i.e., $\alpha_s=0.7+7.5\times10^{-2}\mathcal{P}$, where $\mathcal{P}$ is in units of 10^{-7} torr, and the dashed line is the best linear fit for D_2, i.e., $\alpha_s=0.3+4\times10^{-2}\mathcal{P}$ (Fig. 4). The interaction of the beam with the gas leads mainly to the production of M_2^+ and M^+, where M is H or D, in a ratio 1:0.1 [7] or 1:0.17, according to more recent measurements [8].

Direct recombination, which occurs with secondary electrons since their energy is much less than that of the electron beam, should give a pressure dependence $P^{1/2}$ far from that observed. For the sake of simplicity, we neglect M^+ compared with M_2^+. Moreover, we consider two loss channels for M_2^+, i.e, recombination with secondary electrons, whose density is $N_{es}=N(M_2^+)+N(M_3^+)$, and formation of the ionized compound M_3^+ by collisions with M_2, while the main decay channel of M_3^+ is simply due to recombination with secondary electrons.

Since the degree of ionization is very low (Fig. 4), we solve the stationary rate equations for M_2^+ and M_3^+

neglecting terms containing $N_{es}M_2^+$ and $N_{es}M_3^+$ compared with terms depending on $M_2M_2^+$. Hence we obtain

$$M_2^+ = \frac{\sigma_0 v_{0p} n_{0p}}{\sigma_3 v_2 \left[1+\frac{\sigma_{R2}}{\sigma_{R3}}\right]} , \quad M_3^+ = \frac{\sigma_3 v_2 N_G}{2\sigma_{R3} v_{es}} \tag{22}$$

and hence

$$\alpha_s = \frac{\sigma_0 v_{0p}}{\sigma_3 v_2 \left[1+\frac{\sigma_{R2}}{\sigma_{R3}}\right]} + \frac{\sigma_3 v_2 N_G}{2\sigma_{R3} v_{es} n_{0p}} , \tag{23}$$

where σ_0, σ_3, σ_{R2}, and σ_{R3} represent the cross sections of electron-impact ionization of M_2, of formation of M_3^+ by collision $M_2^+ + M_2$, whose relative velocity is v_2, and of recombination of M_2^+ and M_3^+ with secondary electrons, whose velocity is v_{es}, respectively. N_G is the gas density.

Unfortunately, not all values concerning the involved cross sections are at present available in the literature especially for D_2. Moreover, some data differ from each other for a factor of about 3 or more especially with regards to the recombination cross sections.

We evaluate the coefficients of Eq. (23) for H_2 assuming $\sigma_0 \approx 1$ Å^2 [5,6], $\sigma_3 \approx 76$ Å^2 [9], $\sigma_{R2} \approx 15$ Å^2 [10] and $\sigma_{R3} \approx 3$ Å^2 [10], for the estimated temperature of secondary electrons $T_{es} = 2$ eV. Then, the values of first and second term are ≈ 6 and $\approx 1.3 \times 10^{-2}$, respectively, whereas the best fit gives 0.7 and 7.5×10^{-4}, respectively, where the angular coefficient is converted in units of N_G dividing by 100. A different choice of the cross section values leads to no significant reduction of the gap between calculated and best-fit coefficients.

For instance, different values for σ_3 were measure in the experiments of Refs. [11] and [12], i.e., 51 Å^2 and 29 Å^2, respectively. Moreover, Peart and Dolder report on recombination cross sections, i.e., $\sigma_{R2} \approx 3$ Å^2 [13], and $\sigma_{R3} \approx 6$ Å^2 [14], quite different from values of Ref. [10] especially for the ratio σ_{R2}/σ_{R3}. Then, assuming the lowest and highest value for σ_3 and σ_{R3}, i.e., 29 Å^2 and 6 Å^2, respectively, the second term is reduced by a factor of 5, whereas the first one increases by a factor of 10. Therefore, this disagreement cannot be ascribed to an unperfect knowledge of the cross sections.

A partial explanation can be given in the framework of collective effects. In fact, the rate of processes can be modified by the self-generated field, which affects the energy of reactants. Then, in principle, coefficients of Eq. (23) depend on the gas pressure, i.e., on the degree of ionization.

First of all, the secondary electron temperature T_s depends on the thermal expansion as $T_{0s} f_s^{2/3} = T_{0s}(T_{0p}/T_{0s})^{2/5} f_p^{2/3}$ (Sec. III). Hence the effective temperature, at $P = 10^{-8}$ torr, is $T_s \approx 0.08$ eV. Taking into account that σ_{R3} scales approximately as T_s^{-1} [10,13,14], the recombination rate is about a factor of $(T_{0s}/T_s)^{1/2} \approx 5$ greater than that calculated above. At $P = 10^{-4}$ torr, $T_S \approx 0.5$ eV because of the focusing, and hence $(T_{0s}/T_s)^{1/2} \approx 2$.

Let us now evaluate the effective ion energy, and the rate of H_3^+ formation. An estimation of the σ_3 dependence on the energy of reactants can be extrapolated from data of Ref. [12], even though authors studied the reaction $H^+ + D_2$. Then σ_3 scales approximately as E^{-1}, and the rate of $E^{-1/2}$.

The collective ion kinetic energy, in the coupled region defined by Eq. (9), is given by integration of Eq. (3) under stationary conditions, i.e.,

$$U_i(r) = kT_i + 2\pi e^2 n_{0p}[\alpha_s(1-f_s)-f_p]r^2 \tag{24}$$

whose maximum value occur for $r = r_{\lim}$. It is convenient to represent the H_3^+ formation as a function of the thermal rate calculated above, i.e.,

$$\sigma_3 v_2 = [\sigma_3 v_2]_{\text{th}} \frac{1}{\left[1+\frac{br^2}{kT_i}\right]^{1/2}} , \tag{25}$$

where $b = 2\pi e^2 n_{0p}[\alpha_s(1-f_s)-f_p]$. The average value of Eq. (25) in the coupled region is given by

$$\sigma_3 v_2 = [\sigma_3 v_2]_{\text{th}} \left[\frac{kT_i}{br_{\lim}^2}\right]^{1/2} \times \ln\left[\left[\frac{br_{\lim}^2}{kT_i}\right]^{1/2} + \left[1+\frac{br_{\lim}^2}{kT_i}\right]^{1/2}\right] . \tag{26}$$

From the above data, it results $\sigma_3 v_2 \approx [\sigma_3 v_2]_{\text{th}}$ for $P = 10^{-8}$ torr, with $br_{\lim}^2 \approx 0.4$ eV, and $\sigma_3 v_2 \approx 0.17\,[\sigma_3 v_2]_{\text{th}}$ for $P = 10^{-4}$ torr, with $br_{\lim}^2 \approx 40$ eV.

Taking into account collective effects, it turns out that the value of the angular coefficient of Eq. (23) becomes $\approx 2.6 \times 10^{-3}$ quite close to that deduced from the best fit (7.5×10^{-4}), and barely dependent on pressure, because the rates of H_3^+ formation and recombination exhibit a similar decrease as a function of pressure. Nevertheless since $\sigma_3 v_2 \approx [\sigma_3 v_2]_{\text{th}}$ for $P = 10^{-8}$ torr, the constant term of Eq. (23) is not modified by collective effects. However, at present, no detailed data are available about the σ_3 behavior in the energy interval 0–0.4 eV, which could be less than E^{-1}. In this case, assuming $\sigma_3 v_2 \propto E^{1/2}$, we obtain an overestimation of the rate of H_3^+ formation, whose mean value, in the range $0-r_{\lim}$, becomes $\sigma_3 v_2 \approx 3[\sigma_3 v_2]_{\text{th}}$ for $P = 10^{-8}$ torr. In this case, the constant term of eq. (23) approaches better the value of the best fit.

Note that, in the pressure range 10^{-8}–10^{-6} torr, the value of $\sigma_3 v_2 \approx 3[\sigma_3 v_2]_{\text{th}}$ is quite constant, and the second term of Eq. (23) is negligible. In the region 10^{-8}–10^{-6} torr, a nonperfect agreement with the linear fit may depend on the weak variation of coefficients of Eq. (23) with pressure.

As pressure increases further, the first term becomes negligible compared with the second one, whose coefficient becomes approximately constant. By the way, the constant term of Eq. (23) scales as $E_p^{1/2}$, what is confirmed by measurements with 40-eV beam energy.

Although consistent, the theoretical values of coefficients of Eq. (23) are systematically greater than those deduced from the experimental data. Since σ_0 should be not affected by collective plasma interactions for a beam electron energy 100 eV, it could indicate an underestimation, in the rate equation model, of loss channels for both H_2^+ and H_3^+, as for instance formation of H_5^+ [13] by collision $H_3^+ + H_2$, and by H_2^+ collision with neutral long-lived highly excited H_3. On the other hand, very large recombination rates were found in equilibrium plasmas [15], close to our experimental situation, probably due to the interference among several decay channels, and modifications of reactant energy induced by the self-generated electric field.

From the above discussion, it turns out that plasma effects play a role at a very low charge density, namely $\approx 3\times 10^7$ electrons/cm^3. Hence, plasma, although tenuous, seems a not convenient tool to measure cross sections of elementary processes [16]. The ratios between the best-fit coefficients for H_2 and for D_2 are 2.33 and 1.88, respectively, with a confidence of 40%. Since σ_0 does not depend on the gas [5], taking into account the different velocities of ions due to the mass, after rearrangement we obtain $\langle\sigma_{R2}+\sigma_{R3}\rangle_D/\langle\sigma_{R2}+\sigma_{R3}\rangle_H = 5\pm 2$ and $(\langle\sigma_3\rangle_D/\langle\sigma_3\rangle_H(\langle\sigma_{R3}\rangle_H/\langle\sigma_{R3}\rangle_D) = 0.6\pm 02$.

A ratio less than 2 between the total recombination cross sections of H_2^+ and D_2^+ can be inferred from data of Refs. [10 and [13]. Anyway, assuming that the total recombination ratio is equal to the recombination ratio of H_3^+ and D_3^+, we obtain $\langle\sigma_3\rangle_D/\langle\sigma_3\rangle_H = 3\pm 2$. Actually, an indirect confirmation of a higher value of D_3^+ formation cross section is given in Ref. [17], where the D_3^+ and H_3^+ formation through high-lived autoionizing states has been investigated. In this case, the deuterium cross section that results is two times the hydrogen one.

Figure 5 shows the experimental behavior of I_T in the case of diffuse gas and gas injected by the needle. We

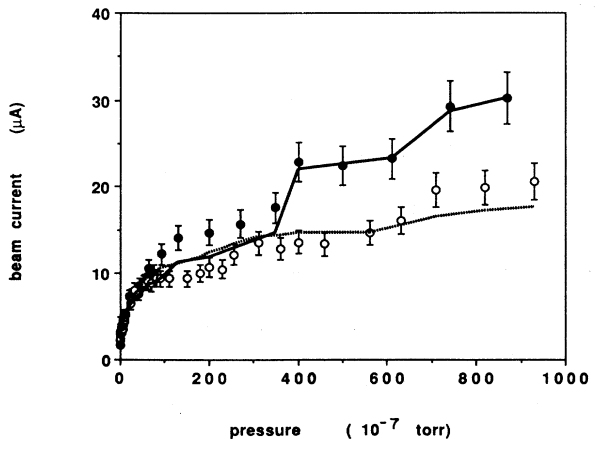

FIG. 5. I_T vs D_2 pressure. Electron-beam energy 100 eV. (a) Open circles, experimental data for diffuse gas. (b) Black circles, experimental data for gas injected by needle. Solid and dashed lines are the fits for gas injected by needle and diffuse gas, respectively.

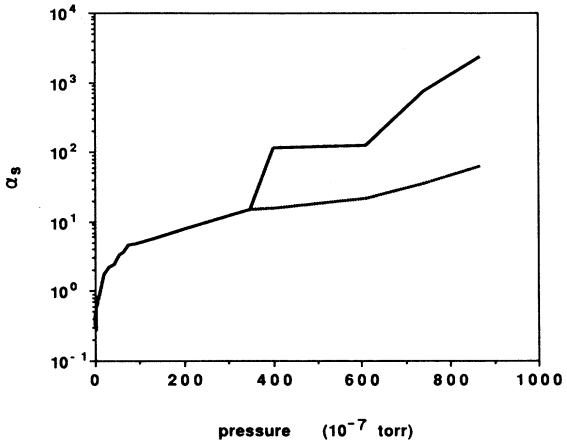

FIG. 6. Ratio α_s between the produced charge density and the electron-beam density $n_{0p} = 4\times 10^7$ electrons/cm^3 vs pressure in D_2. Electron-beam energy 100 eV. Solid and dashed lines correspond to gas injected by needle and to diffuse gas, respectively.

choose a linear scale for the horizontal axis in order to emphasize the needle contribution, which begins to be important at a pressure of about 2×10^{-5} torr. The dashed line is the same fit of Fig. 2, while the solid line has been obtained by using data for diffuse gas in Eqs. (20) and (21), which represent the needle contribution. Figure 6 shows the α_s dependences on the gas pressure from which we estimate the needle overpressure in the region of linear dependence, i.e., ten times the background pressure with a confidence of 20%.

Note that the needle contribution begins to be effective at a background pressure approximately corresponding to the ratio between the needle radius and the distance between the electron gun and the detector times the needle overpressure. Actually, the contribution to the self-consistent electric field, due to the additional ionization, occurs only in the needle region.

V. CONCLUSIONS

In the past little attention was paid to the focusing of a continuous electron beam compared with the pulsed regime where strong increase of the axial beam current occurs [2,18,19]. In Refs. [18] and [19], authors observed strong focusing during the injection of a nonrelativistic electron beam (≈ 2 keV) in a low-density gas (10^{-4} torr). In this case, during the transient stage, the axial beam current is far greater than that measured in a steady-state regime, which occurs some microseconds after the beam switching occurs. Whereas the transient behavior is rather independent of the distance between detector and electron gun, the steady-state current decreases quadratically as a function of the distance [18], in agreement with the focusing condition given by Eq. (19). Moreover, maximum steady-state current was observed up to ≈ 15 cm from the electron gun, a value deduced from Eq. (19) taking into account degree of ionization ($\approx 5\times 10^9$ electrons/cm^3), and beam energy (≈ 2 keV) in the experiments of Refs. [18] and [19]. As a consequence of ion

diffusion, and of the neutralization of the self-generated field by secondary electrons, steady state has been considered a regime not convenient in order to reduce divergence of electron beams [18,19].

Initially, we considered measurements in the continuous regime as a diagnostic support for a pulsed electron-impact ionization experiment in D_2 and H_2 similar to that of Ref. [2]. In fact, our first aim was simply to carry out the maximum electron-beam density n_{0p}, which plays a crucial role in electron and ion focusing [1–4]. Nevertheless, a glance to data of Figs. 2 and 3 showed that n_{0p} could not be directly calculated from the measured current. In fact, from the maximum value of I_d and I_T (Figs. 2 and 3) and assuming a uniform distribution, we obtain $n_{0p} \approx 4 \times 10^6$ electrons/cm^3 and $n_{0p} \approx 4 \times 10^4$ electrons/cm^3, respectively. It indicates a not surprising nonuniform radial density distribution. Hence we could accept $n_{0p} \approx 4 \times 10^6$ electrons/cm^3, deduced from I_d, as a value close to the maximum. Unfortunately, since the radial distribution is unknown and I_d is not completely saturated, this value is affected by a large incertitude. Indeed, the value, deduced from the experimental results by using the model of Sec. III, is one order of magnitude greater. Therefore, in order to use the continuous beam focusing as a diagnostic method, it was necessary to understand, and hence quantitatively describe, the involved phenomena.

As demonstrated in Sec. IV, the three-fluid approach, which describes the time-space evolution of Gaussian-shaped charge-density distributions [1–4], can be successfully applied also in the stationary phase, providing that ions be assumed at rest. It leads to Eq. (19) which gives the spatial scale, as a function of beam and gas parameters, where focusing of a continuous electron beam occurs. Moreover, as a consequence of Eq. (19), the use of gas injected by a needle seems *a posteriori* an attractive method to achieve high focusing of a continuous electron beam, which deserves further investigations, especially in view of applications.

Finally, the behavior of the ionization as a function of the pressure gives information about the elementary processes, and the influence of collective effects. Moreover, the maximum value of f_p, if achieved, provides an indirect evaluation of the temperature of secondary electrons. Then the method can be considered a complementary, quite simple, diagnostic of quasiequilibrium plasmas. Tests with different gases should be convenient to ascertain the applicability of this technique.

ACKNOWLEDGMENT

This work was partially supported by the Consiglio Nazionale delle Ricerche.

[1] F. Giammanco, Phys. Rev. A **40**, 5160 (1989).
[2] F. Giammanco, G. Arena, R. Bruzzese, and N. Spinelli, Phys. Rev. A **41**, 2144 (1990).
[3] F. Giammanco, Phys. Rev. A **40**, 5171 (1989).
[4] F. Giammanco, Phys. Rev. A **43**, 6939 (1991).
[5] D. Rapp and P. Englander-Golden, J. Chem. Phys. **43**, 1464 (1965).
[6] I. R. Cowling and J. Fletcher, J. Phys. B **6**, 665 (1973).
[7] D. Rapp, P. Englander-Golden, and D. D. Briglia, J. Chem. Phys. **42**, 4081 (1965).
[8] H. Kossmann, O. Schwarzkopf, and V. Schmidt, J. Phys. B **23**, 301 (1990).
[9] D. Van Pijkeren, E. Boltjes, J. Van Eck, and A. Niemaus, Chem. Phys. **91**, 293 (1984).
[10] A. Auerbach, R. Cacak, R. Caudano, T. D. Gaily, C. J. Keyser, J. W. McGowan, J. B. A. Mitchell, and S. F. J. Wilk, J. Phys. B **10**, 3797 (1977).
[11] I. Koyano and K. Tanaka, J. Chem. Phys. **72**, 4858 (1980).
[12] S. L Anderson, S. A. Houle, D. Gerlich, and Y. T. Lee, J. Chem. Phys. **75**, 2153 (1981).
[13] B. Peart and K. T. Dolder, J. Phys. B **7**, 236 (1974).
[14] B. Peart and K. T. Dolder, J. Phys. B **7**, 1948 (1974).
[15] M. T. Leu, M. A. Biondi, and R. Johnsen, Phys. Rev. A **8**, 413 (1973).
[16] F. P. Yousif, P. J. T. Van der Donk, M. Orakzai, and J. B. A. Mitchell, Phys. Rev. A **44**, 5653 (1991).
[17] V. Berardi, N. Spinelli, R. Velotta, M. Armenante, and A. Zecca, Phys. Rev. A **47**, 986 (1993).
[18] V. P. Kovalenko and S. F. Fastovets, Fiz. Plazmy **9**, 964 (1983) [Sov. J. Plasma Phys. 9 (5), 562 (1983)].
[19] G. I. Guseva and M. A. Zav'yalov, Fiz. Plazmy **13**, 366 (1987) [Sov. J. Plasma Phys. **9**, (4), 445 (1987)].